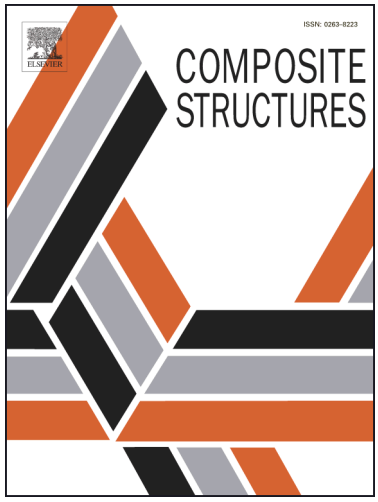

Thermal effect on the pull-in instability of functionally graded micro-beams subjected to electrical actuation

X.L. Jia, S.M. Zhang, L.L. Ke, J. Yang, S. Kitipornchai

PII: S0263-8223(14)00204-9
DOI: http://dx.doi.org/10.1016/j.compstruct.2014.05.004
Reference: COST 5682

To appear in: *Composite Structures*

Please cite this article as: Jia, X.L., Zhang, S.M., Ke, L.L., Yang, J., Kitipornchai, S., Thermal effect on the pull-in instability of functionally graded micro-beams subjected to electrical actuation, *Composite Structures* (2014), doi: http://dx.doi.org/10.1016/j.compstruct.2014.05.004

Thermal effect on the pull-in instability of functionally graded micro-beams subjected to electrical actuation

X. L. Jia[1*], S. M. Zhang [1], L. L. Ke[2], J. Yang [3], S. Kitipornchai[4]

[1] College of Mechanical and Transportation Engineering, China University of Petroleum-Beijing, 18 Fuxue Road, Changping, Beijing, CO 102249, China
[2] Institute of Engineering Mechanics, Beijing Jiaotong University, Beijing 100044, China
[3] School of Aerospace, Mechanical and Manufacturing Engineering, RMIT University, PO Box 71, Bundoora, VIC 3083 Australia
[4] School of Civil Engineering, The University of Queensland, Brisbane, St Lucia 4072, Australia

Abstract. The thermal effect on the pull-in instability of functionally graded micro-beams under the combined electrostatic force, temperature change and Casimir force is studied based on Euler-Bernoulli beam theory and von Kármán geometric nonlinearity. Take into consideration the temperature-dependency of the effective material properties, the Voigt model and exponential distribution model is used to simulate the material properties of the functionally graded materials (FGMs). Principle of virtual work is used to derive the nonlinear governing differential equation which is then solved using the differential quadrature method (DQM). A parametric study is conducted to show the significant effects of material composition, temperature change, geometric nonlinearity and Casimir force.

Keywords: Functionally graded materials; Micro-beam; Temperature change; Pull-in instability; Casimir force

*Corresponding author, Ph. D, E-mail address: xljia@cup.edu.cn
Tel: +86 10 89733762

1. Introduction

Micro-Electro-Mechanical Systems (MEMS) can be defined as systems of small dimensions fulfilling a smart function. The devices are typically designed to operate in one or more energy domains due to their unique advantages such as small size, lower power consumption, lower operation cost, increased reliability and higher precision. With MEMS are used more and more widely due to their unique advantages, such as small size, lower power consumption, lower operation cost, increased reliability and higher precision, numerous analytical, numerical and experimental studies have been conducted on the pull-in instability of the MEMS devices [1-5].

Most recently, the use of functionally graded materials (FGMs) in MEMS structures has been proposed by Craciunescu and Wuttig [6] and Fu *et al.* [7], since FGMs offer many advantages including improved stress distribution, enhanced thermal resistance, higher fracture toughness, and reduced stress intensity factors that make them very attractive in many engineering applications [8]. Specially, Witvrouw and his co-workers [9, 10] developed a multilayer poly-SiGe deposition process for fabricating MEMS structural layers that fulfill all material and economical requirements.

Along with the development of technology, MEMS are expected to be used in high temperature environments. Therefore, the properties of functionally graded MEMS devices under the combined electrostatic force and temperature change are badly in need of investigation. Carbonari *et al*. found that the material gradient played an important role in improving actuator performance, which could also lead to optimal displacements and coupling ratios with reduced amount of piezoelectric material [11]. Hasanyan *et al.* discussed the pull-in instabilities of functionally graded MEMS due to the heat generated by an electric current; it was found that the pull-in voltage can be regulated by varying volume fractions of two constituents through the thickness of a functionally graded plate [12]. Jia *et al.* studied the pull-in instability and free vibration of electrostatically actuated FGM micro-beams allowing for the geometric nonlinearity and intermolecular Casimir force, but without considering the temperature change [13-16]. Mohammadi-Alasti *et al.* investigated the mechanical behavior of a cantilever FGM micro-beam subjected to a nonlinear electrostatic pressure and a temperature change. Their study showed that a temperature change resulted in the deflection of FGM micro-beam due to the variable thermal expansion coefficient along the thickness [17]. The mechanical behavior of FGM micro-tweezer under DC voltage and temperature variations is investigated by Rezaee *et al.* [18]; it is found that increase the ceramic percentage increases the system equivalent stiffness. However, two important factors, i.e. geometric nonlinearity and intermolecular force were neglected in their analysis.

The differential quadrature method (DQM) for the solution of linear and nonlinear differential equations was first introduced by Bellman et al. [19]. Jang extended DQM to the nonlinear analysis of structural components, where the δtechnique was proposed to eliminate the difficulties in implementing two conditions at a single boundary point [20]. Wang et al. [21] gave a new approach to apply the DQM to the deflection, buckling, and free vibration analysis of beams and plates with various boundary conditions. A generalized and more complete methodology for treating boundary conditions in the DQM is presented by Chen et al. [22]. Moreover, there are new ways of implementing the boundary conditions without using δtechnique. The most known is the GDQ Rule (GDQR), in which the rotations are included as unknowns in the displacement vector. Using GDQR, Liu et al. investigated the free vibration of multispan and stepped Euler beams, and beams carrying an intermediate or end concentrated mass[23]. The GDQR techniques were first applied to both spatial and time dimensions simultaneously as a whole by Wu et al. to study the forced vibration of structural beams [24].

Recently, many studies have been carried out on the mechanical behaviors of FGM beams and plates using DQ method. Wu et al. investigated the dynamic stability of thick functionally graded material plates subjected to aero-thermo mechanical loads [25]. The effects of three-parameter

elastic foundations and thermo-mechanical loading on axisymmetric large deflection response of a simply supported annular FGM plate are discussed by Sepahi et al. [26]. Komijani et al. given an analysis of buckling and post-buckling and small amplitude vibrations in the pre/post-buckling regimes of functionally graded beams resting on a nonlinear elastic foundation and subjected to inplane thermal loads [27].

This paper investigates the pull-in instability of fixed FGM micro-beams under a combined action of electrostatic force, temperature change and Casmir force within the framework of von Karman nonlinearity and Euler-Bernoulli beam theory. The temperature-dependency of the effective material properties is specially considered. The nonlinear pull-in results of the micro-beam are obtained by using the DQM. The effects of temperature change, material composition, geometrical nonlinearity and Casimir force are discussed in detail through a parametric study. To the authors' best knowledge, no previous studies which cover all these issues are available.

2. FGM beam model

Figure 1(a) [15] shows the structure of a typical MEMS device, e.g., a micro-switch, where the key components include a fixed electrode modeled with curved upper face as a ground plane and a movable upper electrode modeled as a FGM micro-beam with length L, width b, and thickness h, separated by a dielectric spacer with an initial gap $g_0(x)$. The origin of the x-coordinate is taken to be the left end of the movable electrode whose deflection is denoted by w. The deflection of the micro-beam is caused by the electrostatic force induced by an applied voltage, intermolecular Casimir force and temperature change.

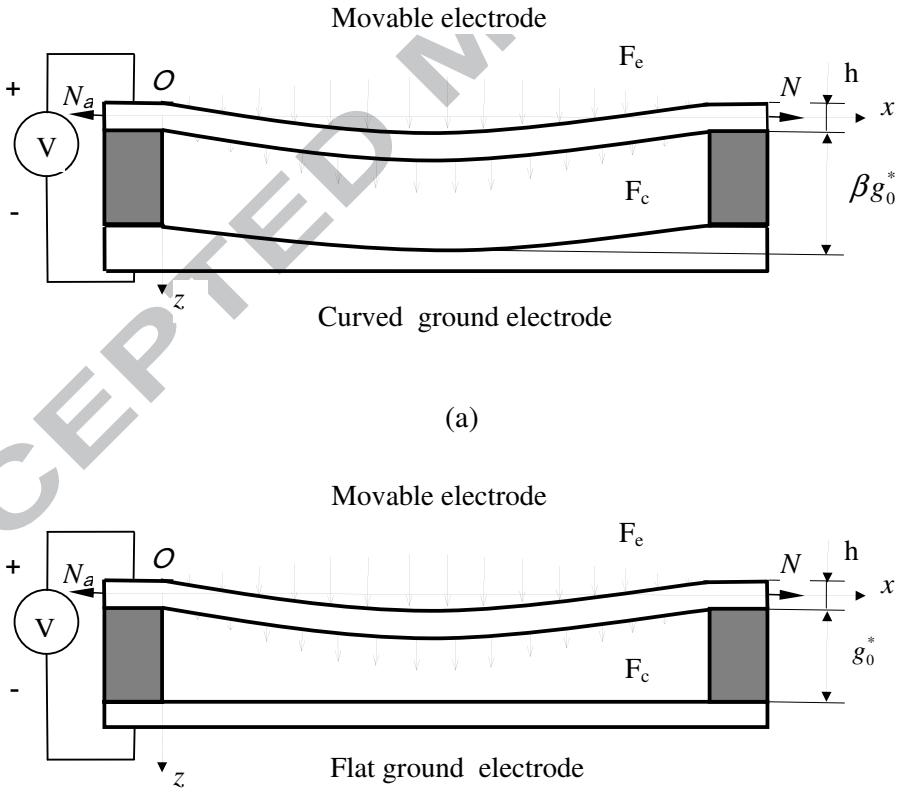

Figure 1. A beam model for the MEMS device: (a) Fixed-fixed micro-beam with curved ground electrode ($\beta > 0$, $\beta \neq 1$); (b) Fixed-fixed micro-beam with flat ground electrode ($\beta = 1$).

Without the loss of generality, the curved upper face of the ground electrode is assumed to be a symmetrical second-order polynomial shape [28] in this paper. Hence, the initial gap is expressed as

$$g_0(x) = g_0^*\left[1 + \frac{4(\beta-1)}{L^2}\left(Lx - x^2\right)\right], \tag{1}$$

where g_0^* denotes the gap distance at fixed ends $x = 0$ and $x = L$; β is the ground electrode shape parameter characterizing the ground electrode shape; βg_0^* represents the initial gap at the middle point $x = L/2$, see figure 1(a). As a special case $\beta = 1$ indicates a flat ground electrode and a uniform initial gap along the beam length see figure 1(b) [16]. The variable ground electrode shape curves with different β are shown in figure 2.

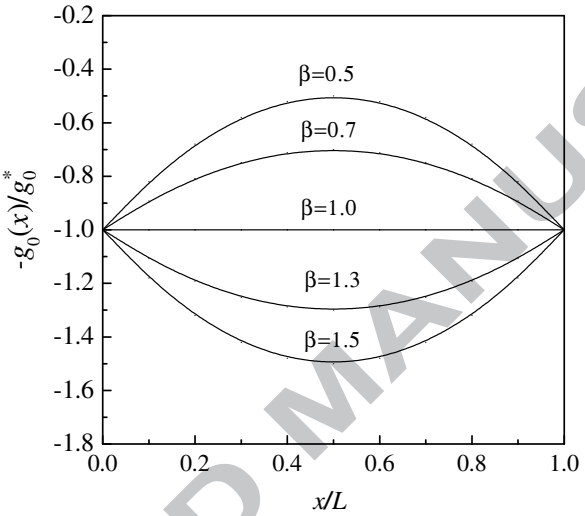

Figure 2. The ground electrode shape curves for different β.

The axial force due to the residual strain from the fabrication process is denoted by N_a and is positive for a tensile force, and vice versa. Under the influence of the temperature change and/or the application of a driving voltage V_0, the micro-beam deflects towards the ground electrode under the action of a distributed electrostatic force F_e, Casmir force F_c and/or thermal strain. Both F_e and F_c are nonlinear functions of the gap $g(x) = g_0(x) - w(x)$ between the deformed micro-beam and the ground electrode.

When the voltage increases beyond a critical value, the movable electrode becomes unstable and collapses to the fixed electrode. This phenomenon, known as pull-in instability, is a subject of prime importance in the design of MEMS devices [29]. In this paper, we define the critical temperature variation when the micro-beam collapses only subjected to the temperature change as the "pull-in temperature variation", and the critical voltage corresponding to the micro-beam under the application of V_0 and temperature change as "pull-in voltage". The pull-in deflection denotes the critical deflection when the micro-beam collapses.

Taking into account the first-order fringing field correction, the electric field force per unit length can be written as

$$F_e = \frac{\varepsilon_0 b V_0^2}{2\left[g_0(x) - w\right]^2} + \frac{0.65\varepsilon_0 V_0^2}{2\left[g_0(x) - w\right]}, \tag{2}$$

where $\varepsilon_0 = 8.854\times10^{-12}\ \mathrm{C^2N^{-1}m^{-2}}$ is the permittivity of vacuum. The Casimir force takes the form of [30, 31]

$$F_c = \frac{\pi^2 \bar{h} c b}{240\left[g_0(x) - w\right]^4} \quad , \tag{3}$$

in which $\bar{h} = 1.055\times10^{-34}$ Js is Planck's constant divided by 2π and $c = 3\times10^{8}$ ms^{-1} is the speed of light.

In this paper, the FGM micro-beam is a mixture of Silicon nitride (Si_3N_4) as material phase 1 whose volume fraction is V_1, and Nickel (N_i) as material phase 2 whose volume fraction is V_2. The mixing ratio changes smoothly and continuously along the thickness direction. The volume fraction of Silicon nitride V_1 and that of Nickel V_2 are given by Reddy [32]

$$V_1 + V_2 = 1, \quad V_2(z) = \left(\frac{2z+h}{2h}\right)^n, \tag{4}$$

where the superscript "*n*" is a power law index that defines the volume fraction profile through beam thickness and can be varied to tailor for desired performance. It is noted that $n = 0$ corresponds to a pure N_i micro-beam. The volume fraction profile thus defined is Si_3N_4-rich at the top beam surface ($z = -h/2$) whereas it is N_i -rich at the bottom surface ($z = h/2$).

According to the Voigt model, the effective material properties P_f of the FGM layer, like Young's modulus E_f, Poisson's Ratio ν_f and thermal expansion coefficient α_f can then be expressed as

$$P_f = \sum_{j=1} P_j V_j \ , \tag{5}$$

where P_j and V_j are the material properties and volume fraction of the constitute material *j*, and

$$\sum_{j=1} V_j = 1 \quad . \tag{6}$$

Since FGM structures are most commonly used in the high-temperature environment, where significant changes in mechanical properties of the constituent materials are to be expected [33], it is essential to take into consideration this temperature-dependency for accurate prediction of the mechanical response. Thus, the effective material properties P_f can be expressed as a nonlinear function of temperature [34]

$$P_j = P_0\left(P_{-1}T^{-1} + 1 + P_1T + P_2T^2 + P_3T^3\right), \tag{7}$$

where P_0, P_{-1}, P_1, P_2 and P_3 are the coefficients of temperature T (in K) and are unique to the constituent materials. Typical values for Si_3N_4 and N_i are list in Tables 1 and 2.

Table 1 Material properties of Silicon nitride (Si_3N_4)

Material property	P_0	P_{-1}	P_1	P_2	P_3
Young's Modulus E(P_a)	348.43×10^{9}	0	-3.070×10^{-4}	2.160×10^{-7}	-8.946×10^{-11}
Poisson's Ratio ν	0.2400	0	0	0	0
thermal expansion coefficient α(K^{-1})	5.8723×10^{-6}	0	9.095×10^{-4}	0	0

Table 2 Material properties of Nickel (N_i)

Material property	P_0	P_{-1}	P_1	P_2	P_3
Young's Modulus $E(P_a)$	223.95×10^{9}	0	-2.794×10^{-4}	-3.998×10^{-9}	0
Poisson's Ratio ν	0.31	0	0	0	0
thermal expansion coefficient $\alpha(\mathrm{K}^{-1})$	9.9209×10^{-6}	0	8.705×10^{-4}	0	0

From equations (4) and (5), one has [35]

$$E_f(z,T)=\left[E_2(T)-E_1(T)\right](0.5+\bar{z})^n+E_1, \tag{8a}$$

$$\alpha_f(z,T)=\left[\alpha_2(T)-\alpha_1(T)\right](0.5+\bar{z})^n+\alpha_1, \tag{8b}$$

$$v_f(z,T)=\left[v_2(T)-v_1(T)\right](0.5+\bar{z})^n+v_1. \tag{8c}$$

3. Theoretical formulations and solution procedures

3.1 Theoretical formulations

It is noted that the ratio h/L is usually small so that the shear deformation is negligible. The total strain at the x direction is the sum of the mechanical strain ε_m and thermal strain ε_T, i.e., $\varepsilon_x=\varepsilon_m+\varepsilon_T$. For micro-beams undergoing moderately large deformation, von Karman type nonlinear strain ε_x is

$$\varepsilon_x=\frac{du}{dx}-z\frac{d^2w}{dx^2}+\frac{1}{2}\left(\frac{dw}{dx}\right)^2, \tag{9}$$

and $\varepsilon_T=\alpha_f(T-T_0)=\alpha_f\Delta T$, where ΔT is the temperature change, measured with respect to the initial temperature T_0. It is noted that this paper takes into account the uniform temperature change.

The strain energy of the micro-beam can be calculated from

$$V=\int_V\int_0^{\varepsilon_x}\sigma_x d\varepsilon_x dV=\int_V\frac{1}{2}E_f\left[\frac{du}{dx}-z\frac{d^2w}{dx^2}+\frac{1}{2}\left(\frac{dw}{dx}\right)^2-\alpha_f\Delta T\right]^2 dV. \tag{10}$$

The total transverse distributed force per unit length $q=F_e+F_c$ is measured positive in the direction of the deflection w and its potential energy is

$$W_q=\int_0^L\left(\int_0^w q\,dw\right)dx=\int_0^L\left[\int_0^w\left[\frac{\varepsilon_0 bV^2}{2(g_0-w)^2}+\frac{0.65\varepsilon_0V^2}{2(g_0-w)}+\frac{\pi^2\bar{h}cb}{240(g_0-w)^4}\right]dw\right]dx. \tag{11}$$

While the potential energy associated with the axial residual stress is

$$W_N=\frac{1}{2}\int_0^L N_a\left(\frac{dw}{dx}\right)^2dx. \tag{12}$$

Based on the principle of virtual work, the governing equations can be expressed as

$$-k_1\left[\frac{3}{2}\left(\frac{dw}{dx}\right)^2\frac{d^2w}{dx^2}+\frac{d^2u}{dx^2}\frac{dw}{dx}+\frac{du}{dx}\frac{d^2w}{dx^2}\right]-k_2\frac{d^3u}{dx^3}+k_3\frac{d^4w}{dx^4}+\left(J_1\Delta T-N_a\right)\frac{d^2w}{dx^2}=q, \tag{13a}$$

$$\frac{d}{dx}\left\{-k_1\left[\frac{du}{dx}+\frac{1}{2}\left(\frac{dw}{dx}\right)^2\right]+k_2\frac{d^2w}{dx^2}\right\}=0. \tag{13b}$$

The associate boundary conditions for fixed beam can be expressed as

$$u=0,\ w=0,\ dw/dx=0 \quad \text{at} \quad x=0 \text{ and } L, \tag{14}$$

in which,

$$k_1=\int_{-\frac{h}{2}}^{\frac{h}{2}}\hat{E}_f b dz,\ k_2=\int_{-\frac{h}{2}}^{\frac{h}{2}}\hat{E}_f b z dz,\ k_3=\int_{-\frac{h}{2}}^{\frac{h}{2}}\hat{E}_f b z^2 dz\ ,\ J_1=\int_{-\frac{h}{2}}^{\frac{h}{2}}\hat{E}_f\alpha_f b dz\ , \tag{15}$$

where the effective modulus $\hat{E}_f=E_f$ for a narrow beam ($b<5h$) and $\hat{E}_f=E_f/\left(1-\nu_f^2\right)$ for a wide beam ($b\geq 5h$). Noted that for a homogenous micro-beam whose Young's modulus is a constant, i.e. $k_2=0$, equation (13) can reduce to the nonlinear governing equations for a homogenous micro-beam.

From equation (13) and boundary conditions (14), the motion equation for an FGM micro-beam subjected to temperature change accounting for the geometric nonlinearity due to the mid-plane stretching can be derived as

$$\left(k_3-\frac{k_2^2}{k_1}\right)\frac{d^4w}{dx^4}+\left(J_1\Delta T-N_a\right)\frac{d^2w}{dx^2}-\frac{d^2w}{dx^2}\int_0^L\left[\frac{k_1}{2L}\left(\frac{dw}{dx}\right)^2-\frac{k_2}{L}\frac{d^2w}{dx^2}\right]dx=q\ . \tag{16}$$

To facilitate theoretical formulation and for generality of solutions, the following dimensionless quantities are introduced

$$k=k_3-k_2^2/k_1\ ,\ \ \psi=\left(J_1\Delta T-N_a\right)L^2/k\ ,\ \ \zeta_1=k_1g_{0m}^2/2k\ ,$$
$$\zeta_2=k_2g_{0m}/k\ ,\ \ \overline{w}_0=w_0/g_{0m}\ ,\ \ \overline{x}=x/L\ , \tag{17}$$

where the maximum initial gap $g_{0m}=\beta g_0^*$ for $\beta\geq 1$, and $g_{0m}=g_0^*$ for $0<\beta<1$. Hence, equation (16) can then be rewritten in dimensionless form as

$$\frac{d^4\overline{w}}{d\overline{x}^4}+\psi\frac{d^2\overline{w}}{d\overline{x}^2}-\frac{d^2\overline{w}}{d\overline{x}^2}\int_0^1\left[\xi_1\left(\frac{d\overline{w}}{d\overline{x}}\right)^2-\xi_2\frac{d^2\overline{w}}{d\overline{x}^2}\right]d\overline{x}=\overline{q}\ . \tag{18}$$

The dimensionless distributed force is

$$\overline{q}(\overline{x})=\frac{R_c}{\left(\overline{g}_0(\overline{x})-\overline{w}\right)^4}+\frac{BV_0^{\ 2}}{\left(\overline{g}_0(\overline{x})-\overline{w}\right)^2}+f\frac{BV_0^{\ 2}}{\left(\overline{g}_0(\overline{x})-\overline{w}\right)}, \tag{19}$$

in which $\overline{g}_0(\overline{x})=\frac{g_0^*}{g_{0m}}\left[1+4\left(\beta-1\right)\left(\overline{x}-\overline{x}^2\right)\right]$, $R_c=\frac{\pi^2\overline{h}cbL^4}{240g_{0m}^5k}$, $B=\frac{\varepsilon_0bL^4}{2g_{0m}^3k}$, $f=0.65\frac{g_{0m}}{b}$. The non-dimensional boundary conditions are $\overline{w}=0,\ d\overline{w}/d\overline{x}=0$ at $\overline{x}=0$ and 1.

3.2 Solution procedures

Equation (18) and the associated boundary conditions form a nonlinear ordinary differential equation system whose exact solution is not available. The DQ method is therefore used to solve this nonlinear system numerically. According to the DQM, the dimensionless deflection $\overline{w}$ and its derivatives at an arbitrary point $\overline{x}_i$ are approximated by [36]

$$\overline{w}=\sum_{j=1}^{N}l_j(x)\overline{w}\left(x_j\right), \tag{20a}$$

$$\left.\frac{d^k\overline{w}}{d\overline{x}^k}\right|_{\overline{x}=\overline{x}_i}=\sum_{j=1}^{N}C_{ij}^{(k)}\overline{w}\left(x_j\right), \tag{20b}$$

where N is the total number of sampling points $\overline{x}_i$ unevenly distributed over the domain[20-22]

$$\overline{x}_1=0.0,\ \overline{x}_2=0.001,\ \overline{x}_j=\frac{1}{2}\left[1-\cos\frac{\pi\left(j-2\right)}{N-3}\right],.....,\ \overline{x}_{N-1}=0.999,\ \overline{x}_N=1.0\ . \tag{21}$$

The weighting coefficients $C_{ij}^{(k)}$ are dependent on the distribution of sampling points only and can be calculated from recursive formulae

$$C_{ij}^{(1)} = \frac{\tilde{L}(\overline{x}_i)}{(\overline{x}_i - \overline{x}_j)\tilde{L}(\overline{x}_j)} \quad i, j = 1,2,\ldots, N;\ i \neq j, \tag{22a}$$

$$C_{ii}^{(1)} = -\sum_{j=1, j\neq i}^{N} C_{ij}^{(1)} \quad i = 1,2,\ldots, N, \tag{22b}$$

$$\tilde{L}(\overline{x}_i) = \prod_{j=1}^{N} (\overline{x}_i - \overline{x}_j) \quad i, j = 1,2,\ldots, N;\ i \neq j. \tag{22c}$$

The higher-order weighting coefficient can then be obtained as follows

$$C_{ij}^{(m)} = m\left[C_{ij}^{(1)} C_{ii}^{(m-1)} - \frac{C_{ij}^{(m-1)}}{\overline{x}_i - \overline{x}_j} \right], \tag{23a}$$

$$C_{ii}^{(m)} = -\sum_{j=1, j\neq i}^{N} C_{ij}^{(m)}, \tag{23b}$$

for $i, j = 1,2,\ldots, N$; $m = 2,3,\ldots, N$-1.

Applying DQ approximations to the governing equation (18), one has

$$\sum_{j=1}^{N} C_{ij}^{(4)} \overline{w}_j + \psi \sum_{j=1}^{N} C_{ij}^{(2)} \overline{w}_j - \sum_{j=1}^{N} C_{ij}^{(2)} \overline{w}_j \sum_{k=1}^{N} \left(C_{Nk}^{I} - C_{1k}^{I} \right) \left(\xi_1 \left(\sum_{j=1}^{N} C_{ij}^{(1)} \overline{w}_j \right)^2 - \xi_2 \sum_{j=1}^{N} C_{ij}^{(2)} \overline{w}_j \right) - \overline{q}_j = 0, \tag{24}$$

in which $\mathbf{C^I} = \left(\mathbf{C^{(1)}}\right)^{-1}$, and the distributed force per unit length can be expressed as

$$\overline{q}_j = \frac{R_c}{\left[\overline{g}_0(\overline{x}_j) - \overline{w}(\overline{x}_j)\right]^4} + \frac{BV_0^2}{\left[\overline{g}_0(\overline{x}_j) - \overline{w}(\overline{x}_j)\right]^2} + f\frac{BV_0^2}{\left[\overline{g}_0(\overline{x}_j) - \overline{w}(\overline{x}_j)\right]}. \tag{25}$$

According to the δtechnique given by Jang [20], the boundary conditions become

$$\overline{w}_1 = 0, \quad \sum_{j=1}^{N} C_{2j}^{(1)} \overline{w}_j = 0, \quad \sum_{j=1}^{N} C_{N-1\,j}^{(1)} \overline{w}_j = 0, \quad \overline{w}_N = 0. \tag{26}$$

It should be noted that discarding the geometrically nonlinear terms in equation (24) leads to the following equations without the effect of geometric nonlinearity

$$\sum_{j=1}^{N} C_{ij}^{(4)} \overline{w}_j + \psi \sum_{j=1}^{N} C_{ij}^{(2)} \overline{w}_j - \overline{q}_j = 0. \tag{27}$$

Denoting the unknown static displacement by $\overline{\mathbf{w}} = \{\overline{w}_i\}^{\mathbf{T}}$ and the transverse force vector by $\overline{\mathbf{q}} = \{\overline{q}_i\}^{\mathbf{T}}$, the nonlinear and linear solutions of pull-in temperature variation ΔT_{PI}, pull-in voltage V_{PI} and pull-in deflection $\overline{w}_{PI}$, when exists, can be determined from equations (24) and (26) and from equations (27) and (26), respectively, following an iterative process below:

(1) Assuming a trial voltage V_0, let $\overline{q}_i = (2\beta + f\beta + 4R_c)\overline{w}_i + \beta + f\beta + R_c \quad (i = 1,2,\ldots N)$, which is the linear part in the Taylor series expansion of $\overline{q}_i$. Solve equation (27) and the associated boundary conditions (26) to find $\overline{\mathbf{w}}$ which is taken as the initial value $\overline{\mathbf{w}}^*$ to be used in the 1st round of iteration.

(2) Substituting $\overline{\mathbf{w}} = \overline{\mathbf{w}}^*$ into equation (25) to obtain a new force vector $\overline{\mathbf{q}}$ and expressing equations (26)-(27) with this updated $\overline{\mathbf{q}}$ in matrix equation yields

$$\mathbf{K}\overline{\mathbf{w}} = \overline{\mathbf{q}}. \tag{28}$$

where $\mathbf{K}$ is the "stiffness matrix". The solution of this equation is denoted as $\overline{\mathbf{w}}^{(1)}$.

(3) Update $\bar{\mathbf{w}}^*$ by $\bar{\mathbf{w}}^* = \bar{\mathbf{w}}^{(1)}$ and repeat step (2) to gain a new solution $\bar{\mathbf{w}}^{(2)}$.
(4) Repeat step (3) until the deflection converges to a prescribed error tolerance

$$\sqrt{\frac{\sum\left(\Delta\bar{\mathbf{w}}^{(k)}\right)^2}{\sum\left(\bar{\mathbf{w}}^{(k+1)}\right)^2}} \le 0.0001. \tag{29}$$

To obtain the linear deflection $\bar{\mathbf{w}}$ under the assumed trial voltage, $\Delta\bar{\mathbf{w}}^{(k)}$ is updated in each iteration by $\Delta\bar{\mathbf{w}}^{(k)} = \bar{\mathbf{w}}^{(k+1)} - \bar{\mathbf{w}}^{(k)}$.
(5) Increase the trial voltage V_0 and repeat steps (1)-(4) until the stiffness matrix $\mathbf{K}$ becomes singular or the iterative process fails to converge. The last trial voltage V_0 under which the deflection is solvable is the linear pull-in voltage V_{PI}, and the corresponding deflection is the linear pull-in deflection $\bar{\mathbf{w}}_{PI}$.
(6) In order to find the pull-in parameters with the effect of geometric nonlinearity, the initial iterative values $\bar{\mathbf{w}}^*$ needs to be put into equation (24) and its relevant boundary conditions. Repeat steps (3)-(5) to obtain the nonlinear pull-in parameters.
(7) Assuming a trial temperature variation ΔT and setting $V_0 = 0$, the "pull-in temperature variation" ΔT_{PI} and the corresponding pull-in deflection can be obtained according to the steps above.

4. Results and discussions

4.1 Validation example

It should be noted that Table 1 and Table 2 list the material properties used in all of the examples except those in Table 3. Besides, the geometric parameters of the micro-beams are L = 410 μm, b = 100 μm, g_0 = 1.18 μm, h = 1.5 μm, unless stated otherwise.

Since there are no experimental results for FGM micro-beams, to validate the present analysis, the linear and nonlinear pull-in voltage results for a homogeneous micro-beam are compared with the experimental results and Ritz method-based solutions provided by Tilmans and Legtenberg [2], in which E = 151GPa, the axial residual force N_a = 0.0009 N. The convergence study is given in Table 3 where the pull-in voltages of clamped micro-beams of different lengths with varying total number of sampling points N are compared. It is seen that convergent results can be achieved when $N \ge 17$ for both linear and nonlinear analyses.

Table 3 Pull-in voltages (in V) of electrostatically actuated homogenous clamped micro-beams

L(μm)	N=13		N=17		N=19		Ritz Method[2]	Experiment [2]
	Linear	Nonlinear	Linear	Nonlinear	Linear	Nonlinear		
210	27.500	28.350	27.506	28.352	27.506	28.352	24.98	27.95
310	13.833	14.181	13.834	14.182	13.834	14.182	11.46	13.78
410	8.769	8.945	8.769	8.945	8.769	8.945	6.55	9.13
510	6.300	6.401	6.300	6.401	6.300	6.401	4.23	6.57

As can be observed in Table 3, compared to the Ritz method the present analysis yields results that are in much better agreement with the experimentally obtained pull-in voltages [2]. The relative difference percentage between the experimental results and our theoretical pull-in voltages increases as the beam length L increases and the percentage reaches 4.1% for L = 510 μm in linear analysis and only 2.6% in nonlinear analysis. This indicates that the geometric nonlinearity due to mid-plane stretching should be taken into account, particularly for long micro-beams [3, 37].

4.2 FGM micro-beam under the influence of uniform temperature change

Figure 3 gives the Young's modulus E_f, Poisson's ratio ν_f and thermal expansion coefficient α_f varying through beam thickness of the 5 different types of FGM micro-beams corresponding to different volume fraction profile (Type1: n=0, Type2: n=0.4, Type3: n=1, Type4: n=5, Type5: n=15). In which, Type 1(n=0) is the pure N_i micro-beam, and Type3 (n=1) represents the beam with two phase N_i and Si_3N_4 linear distributed.

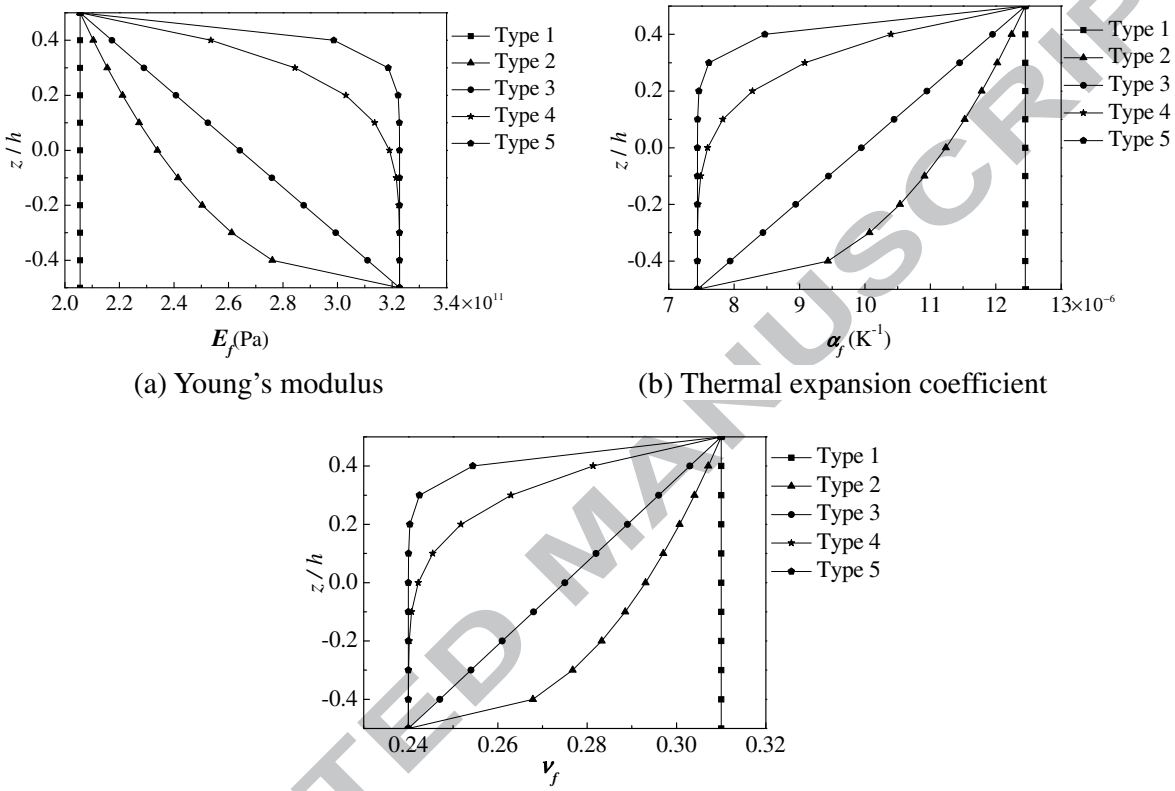

(a) Young's modulus

(b) Thermal expansion coefficient

(c) Poisson's ratio

Figure 3. Young's modulus, thermal expansion coefficient and Poisson's ratio along thickness for the five types of FGM micro-beams.

The effect of uniform temperature change on the pull-in instability of pure N_i (Type 1) and other FGM micro-beams (V=0V) is shown in figure 4, where $\overline{w}_{0\max}$ is the deflection of the middle point of the fixed FGM beam. In this and the following figures, solid lines and dashed lines denote the nonlinear and linear results, respectively. Figure 4 shows that the deflection of the micro-beam increases with the growth of the temperature until a certain value. Then, the deflection increases sharply and the micro-beam loses its stability and spontaneously collapse or pulls in onto the fixed electrode. The micro-beam with a higher value of n has a larger "pull-in temperature variation" ΔT_{PI}, which are (3.55, 4.11, 4.46, 5.16, 5.56) K for Types 1-5, respectively. This is because such a micro-beam contains more N_i whose thermal expansion coefficient is smaller than that of Si_3N_4 (N_i is rich at the bottom). However, the difference between linear and nonlinear results is negligible as shown in figure 4.

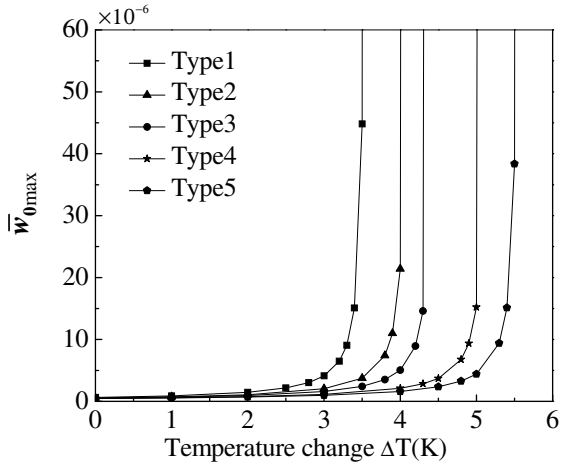

Figure 4. Pull-in instability of functionally graded micro-beams for the five beam types.

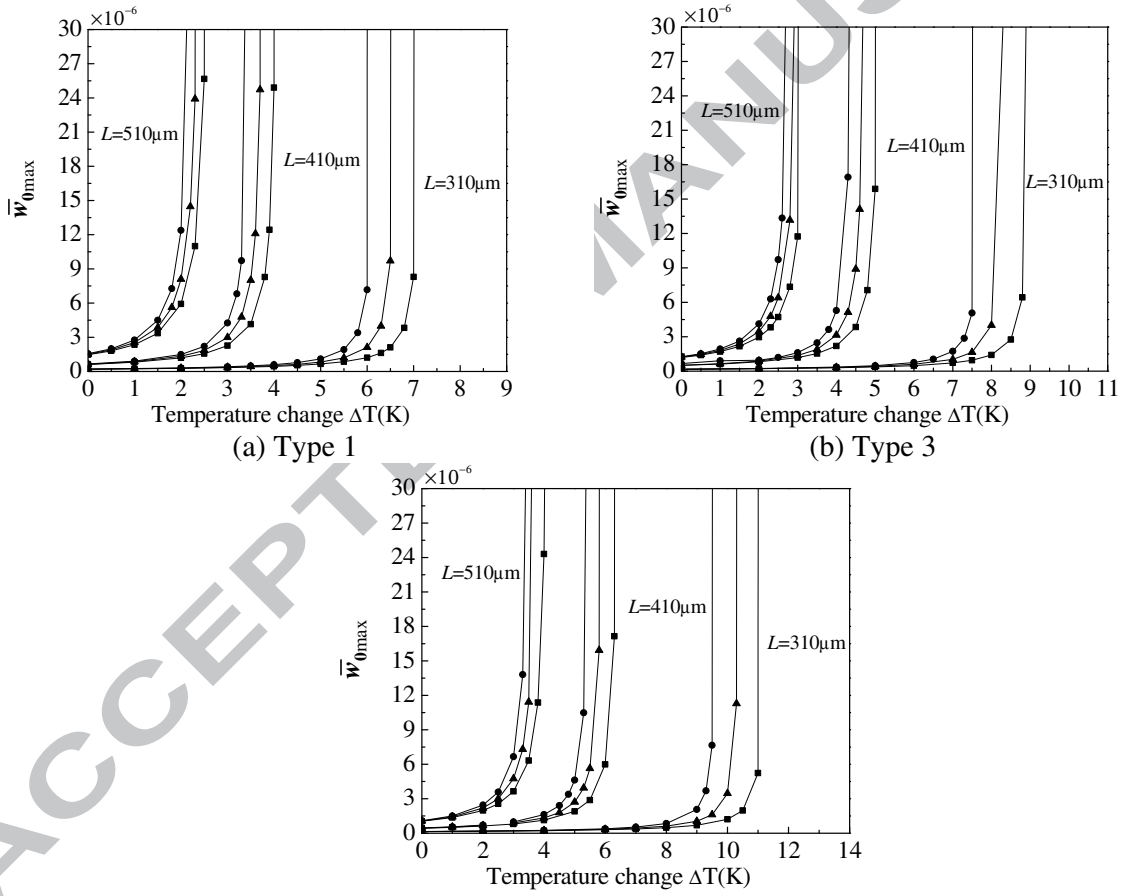

Figure 5. The effect of beam length on the pull-in instability of different beam types.

Plotted in figure 5 and figure 6 are curves showing the effect of beam length and thickness on the curves showing $\overline{w}_{0\max}$ versus the uniform temperature change for different micro-beam types. Where the solid lines with squares, triangle and pentagon represent different temperature T (100K, 200K, 300K) respectively, unless stated otherwise. As expected, the micro-beam with smaller beam length and larger beam thickness has considerably larger "pull-in temperature

variation" ΔT_{PI}. It is noted that the influence of L is more obvious for the beam type with a higher temperature, while the influence of h is more evident in the low-temperature environment.

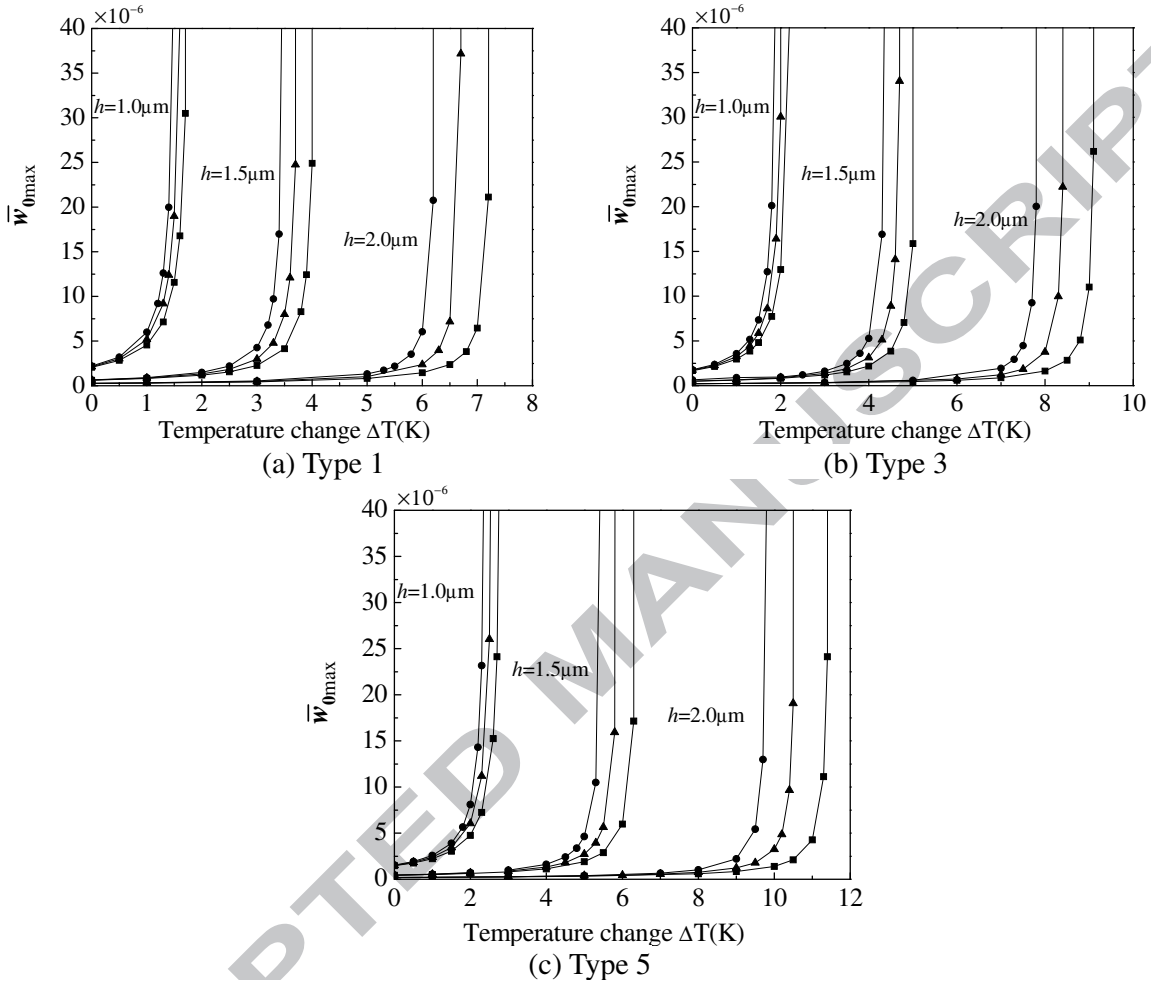

Figure 6. The effect of beam thickness on the pull-in instability of different beam types.

The influence of axial residual force on the pull-in instability of different beam types are dictated in figure 7, where $N_a = 0$ corresponds to a micro-beam without the action of axial residual stress. It is noted that as the axial residual stress N_a changes from a compressive force to a tensile force, the "pull-in temperature variation" ΔT_{PI} increases gradually for all the three beam types. These results imply that a negative axial residual stress can soften while the action of an axial residual tensile force can strengthen the FGM micro-beam. Moreover, this phenomena is more obvious for micro-beams with a lower value of n at higher temperatures.

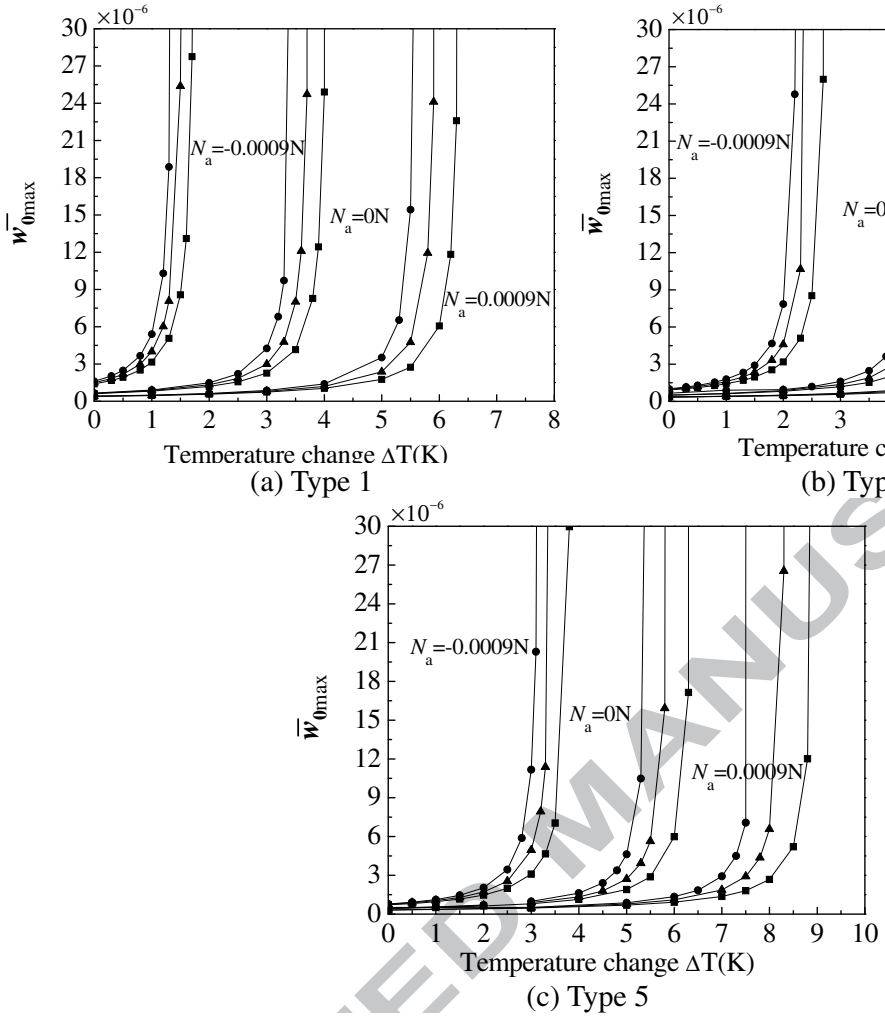

Figure 7. The effect of axial force on the pull-in instability of different beam types.

Figure 8 shows that the effect of ground electrode shape parameter β on the pull-in instability of different beam types is not notable, but the increasing trend of the deflection of the middle point of the fixed FGM beam $\bar{w}_{0\max}$ with the uniform temperature change ΔT is not similar, the micro-beam with a higher β have a sharp growth near the "pull-in temperature variation" ΔT_{PI}.

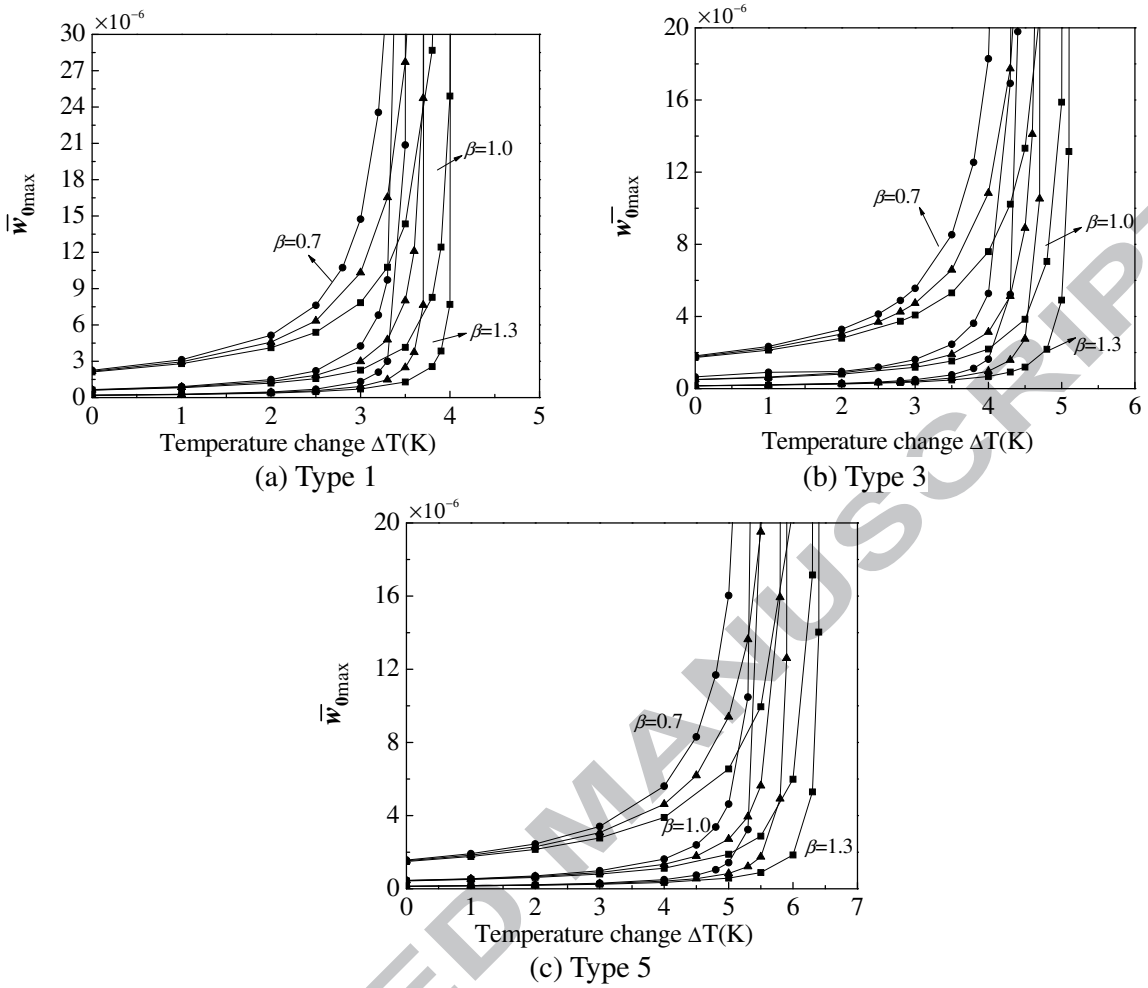

Figure 8. The effect of ground electrode shape parameter on the pull-in instability of different beam types.

In figure 9, the solid lines with hollow squares, triangle and pentagon stands for the micro-beam, in which, N_i-rich at the top beam surface ($z=-h/2$) whereas Si_3N_4-rich at the bottom surface ($z=h/2$). It is shown that the micro-beams N_i-rich at the top beam surface have relative low "pull-in temperature variation" ΔT_{PI}. The effect of the parameters *L, h,* N_a and β on the pull-in instability is similar with that for micro-beam N_i-rich at the bottom surface. Besides, it is noted that under higher temperature, the axial force N_a have obvious effect on increasing ΔT_{PI}.

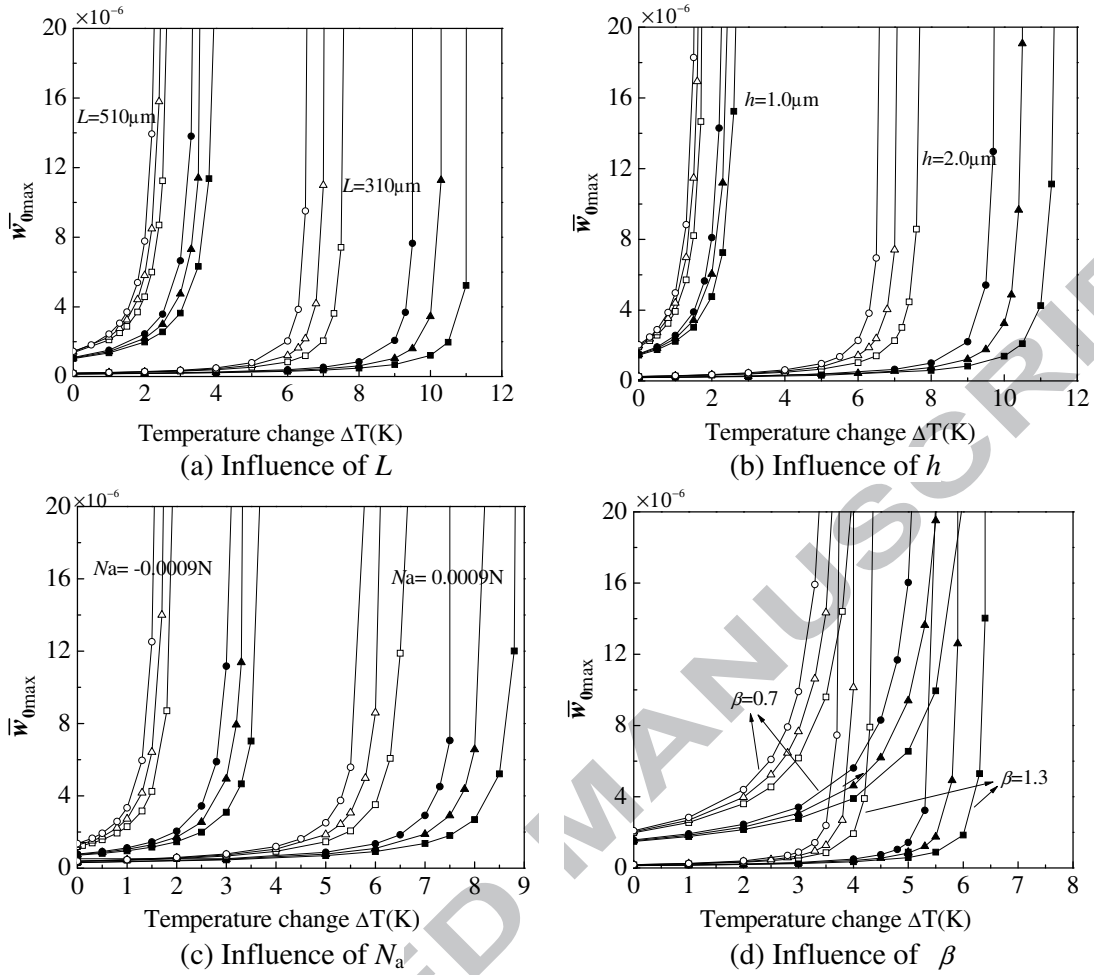

(a) Influence of L (b) Influence of h

(c) Influence of N_a (d) Influence of β

Figure 9. The effect of the main parameter on the pull-in instability of different beam types where N_i-rich at the top beam surface.

4.3 FGM micro-beam subjected to temperature change and nonlinear electrostatic force

Figure 10 depicts the effect of the volume fraction profile parameter on pull-in instability under different temperature conditions. It is noted that the pull-in voltage V_{PI} increase with the growth of the volume fraction profile parameter n and temperature T, while a larger temperature change ΔT leads to a decrease of V_{PI}. Moreover, n exhibits more obvious influence on the pull-in voltage with larger T and ΔT.

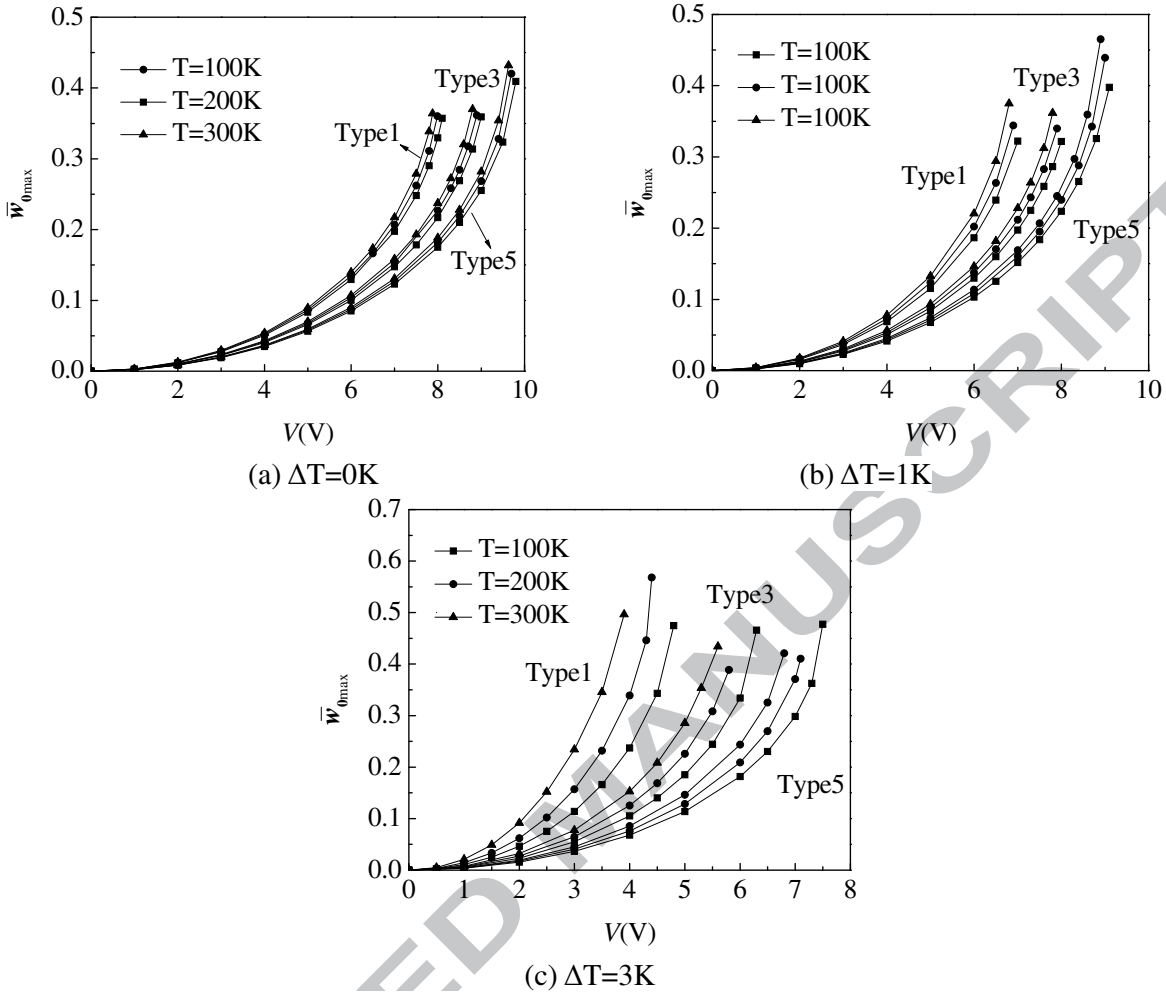

Figure 10. Pull-in instability of different micro-beams subjected to the electrostatic force.

The intermolecular force is of the prominent importance in some micro-switches where the micro-beam may collapse onto the fixed ground plane due to the Casimir force only [37]. Once the stiffness of the micro-beam decrease to some extent, the micro-beam may collapse even in the absence of an applied voltage and temperature change. As an example, we consider a micro-beam with the length $L = 410\mu m$, aspect ratio b/L=0.244 and initial gap $g_0 = 0.5\mu m$. The effect of intermolecular Casimir force on the pull-in instability of different type of FGM micro-beams with varying temperature change ΔT under different temperature T is displayed in figure 11, where the dashed line denotes the results without Casimir force, while the solid line represents the results considering the effect of Casimir force. As can be seen from the results, the neglect of the Casimir force may lead to a considerably underestimated $\bar{w}_{0\max}$. The discrepancy tends to be smaller as the temperature change ΔT decreases and n increases, however, temperature T seems have no influence on the effect of the Casimir force.

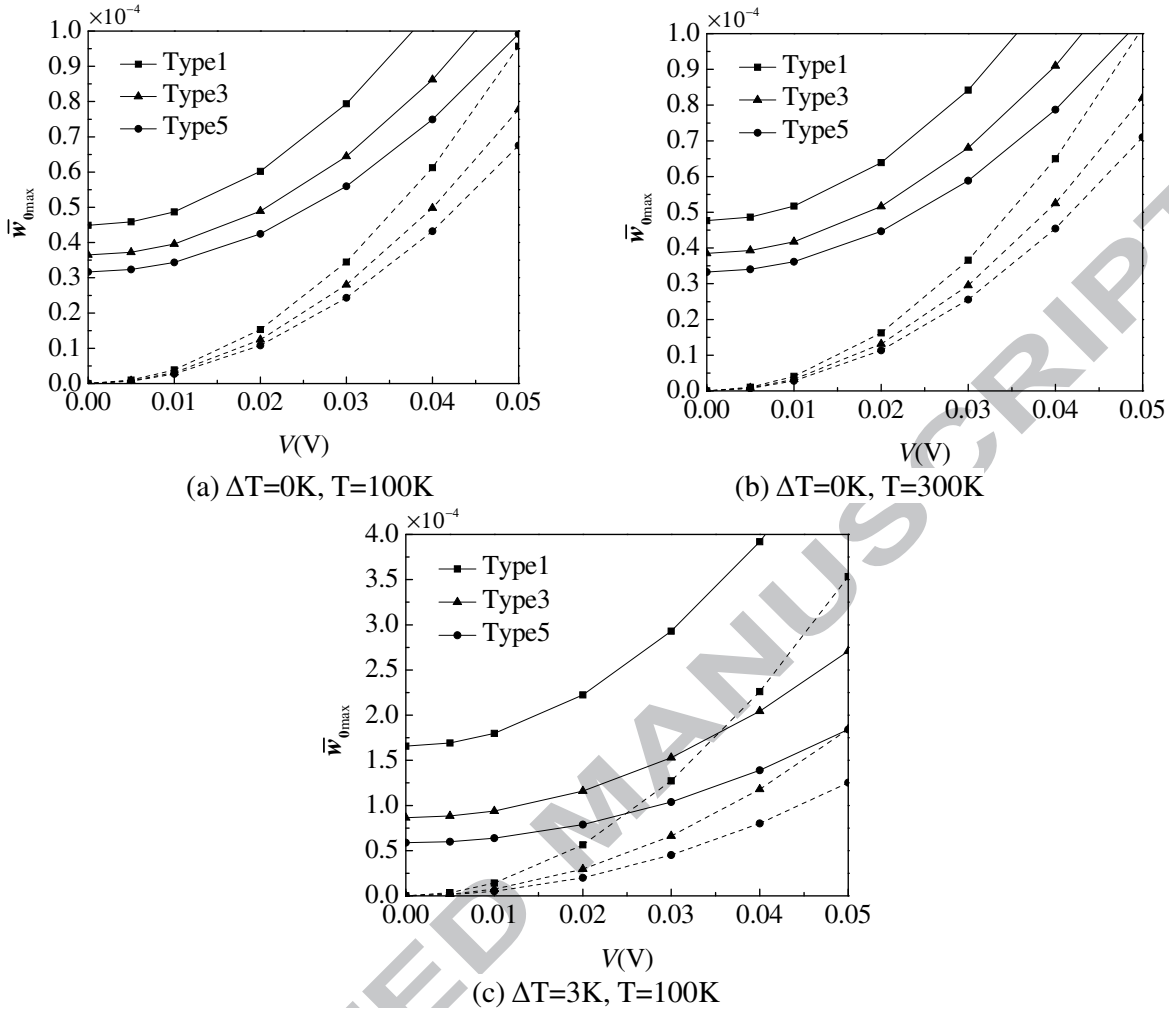

Figure 11. The influence of Casimir force on the pull-in instability of different micro-beams.

5. Conclusions

This paper investigates the pull-in instability of FGM micro-beams under combined electrostatic and intermolecular forces and temperature change. The temperature-dependency of the effective material properties is specially considered. The governing equation and boundary conditions are derived based on Euler-Bernoulli beam theory and von Karman type geometric nonlinearity, then solved numerically through DQ approximation to obtain the "pull-in temperature variation", pull-in voltage and pull-in deflection for fixed micro-beams. A comprehensive study has been conducted to analyze the pull-in instability characteristics, it concluded that:

(1) Taking no account of the electric field force, the FGM micro-beam with a higher volume fraction profile parameter exhibits more obvious thermal expansion phenomenon and can sustain a higher temperature change.

(2) The micro-beam with smaller length and larger thickness has larger "pull-in temperature variation". The influence of the beam length is more obvious for the beam type with a higher temperature, while the influence of the beam width is more evident in the low-temperature environment.

(3) As the axial residual stress changes from a compressive force to a tensile force, the pull-in temperature variation increases gradually for all the three beam types. This phenomenon is more obvious for micro-beams with a lower volume fraction profile parameter at higher temperatures.

(4) The micro-beams N_i-rich at the top beam surface have relative low "pull-in temperature variation" relative to that N_i -rich at the bottom surface.
(5) The pull-in voltage increases with the growth of volume fraction profile parameter and the decease of temperature.
(6) The neglect of Casimir force may lead to a considerably underestimated the deflection of the middle point of the fixed FGM beam. The discrepancy tends to be smaller as the temperature change decreases and volume fraction profile parameter increases.

Acknowledgments

The research described in this paper was financially supported by the Science Foundation of China University of Petroleum, Beijing (No. YJRC-2013-32).

References

[1] Legtenberg R, Tilmans H A C. Electrostatically driven vacuum-encapsulated polysilicon resonators, Part I: Design and Fabrication. Sens Actuators A 1994; 45:57-66.
[2] Tilmans H A C, Legtenberg R. Electrostatically driven vacuum-encapsulated polysilicon resonators, Part II: Theory and performance. Sens Actuators A 1994; 45:67-84.
[3] Abdel-Rahman E M, Younis M I, Nayfeh A H. Characterization of the mechanical behavior of an electrically actuated microbeam. J Micromech Micoreng 2002; 12:759-766.
[4] Batra R C, Porfiri M, Spinello D. Electromechanical model of electrically actuated narrow microbeams. J Microelectromech Syst 2006; 15:1175-1189.
[5] Batra R C, Porfiri M, Spinello D. Vibrations of narrow microbeams predeformed by an electric field. J Sound Vib 2008; 309:600-612.
[6] Craciunescu C M, Wuttig M. New ferromagnetic and functionally graded shape memory alloys. J Optoelectron Adv Mater 2003; 5:139-146.
[7] Fu Y Q, Du H J, Zhang S. Functionally graded TiN/TiNi shape memory alloy films. Mater Lett 2003; 57:2995-2999.
[8] Birman V, Byrd L W. Modeling and analysis of functionally graded materials and structures. Appl Mech Rev 2007; 60:195-216.
[9] Witvrouw A, Mehta A. The use of functionally graded poly-SiGe layers for MEMS applications. Materials Science Forum 2005; 492:255-260.
[10] Gromova M, Mehta A, Baert K, Witvrouw A. Characterization and strain gradient optimization of PECVD poly-SiGe layers for MEMS applications. Sens Actuators A 2006; 130:403-410.
[11] Carbonari R C, Silva E C N, Paulino G H. Multi-actuated functionally graded piezoelectric micro-tools design: A multiphysics topology optimization approach. Int J Numer Methods Eng 2009; 77:301-336.
[12] Hasanyan D J , Batra R C, Harutyunyan S. Pull-in instabilities in functionally graded microthermoelectromechanical systems. J Therm Stresses 2008; 31:1006-1021.
[13] Jia X L, Yang J, Kitipornchai S. Characterization of FGM micro-switches under electrostatic and Casimir forces. IOP Conf Ser: Mater Sci Eng 2010; 10:012018.
[14] Jia X L, Yang J, Kitipornchai S, Lim C W. Free vibration of geometrically nonlinear micro-switches under electrostatic and Casimir forces. Smart Mater and Struct 2010; 19: 115028.
[15] Jia X L, Yang J, Kitipornchai S. Pull-in instability of geometrically nonlinear micro-switches under electrostatic and Casmir forces. Acta Mech 2011; 218:161-174.
[16] Jia X L, Yang J, Kitipornchai S, Lim C W. Pull-in instability and free vibration of electrically actuated poly-SiGe graded micro-beams with a curved ground electrode. Applied Mathematical Modeling 2012; 36:1875-1884.
[17] Mohammadi-Alasti B, Rezazadeh G, Borgheei A M, Minaei S, Habibifar R. On the mechanical behavior of a functionally graded micro-beam subjected to a thermal moment and

nonlinear electrostatic pressure. Compos Struct 2011; 93:1516-1525.
[18] Rezaee M, Sharafkhani N, Chitsaz A. Electrostatically actuated FGM micro-tweezer under the thermal moment. Microsyst Technol 2013; 19:1829-1837.
[19] Bellman R E, Casti J. Differential quadrature and long-term integration. J Math Anal Appl 1971; 34:235-238.
[20] Jang S K. Application of differential quadrature to the analysis of structural components. PhD Thesis, University of Oklahoma, USA; 1987.
[21] Wang X, Bert C W, Striz A G. Differential quadrature analysis of deflection, buckling and free vibration of beams and rectangular plates. Comput Struct 1993; 48:473-479.
[22] Chen W L, Striz A G, Bert C W. A new approach to the differential quadrature method for fourth-order equations. Int J Numer Meth Engng 1997; 40:1941-1956.
[23] Liu G R, Wu T Y. Vibration analysis of beams using the generalized differential quadrature rule and domain decomposition. J Sound Vib 2001; 246:461-481.
[24] Wu T Y, Liu G R, Wang Y Y. Application of the generalized differential quadrature rule to initial-boundary-value problems. J Sound Vib 2003; 264:883-891.
[25] Wu L H, Wang H J, Wang D B. Dynamic stability analysis of FGM plates by the moving least squares differential quadrature method. Compos Struct 2003; 77:383-394.
[26] Sepahi O, Forouzan M R, Malekzadeh P. Large deflection analysis of thermo-mechanical loaded annular FGM plates on nonlinear elastic foundation via DQM. Compos Struct 2010; 92:2369-2378.
[27] Komijani M, Esfahani S E, Reddy J N, Liu Y P, Eslami M R. Nonlinear thermal stability and vibration of pre/post-buckled temperature- and microstructure dependent functionally graded beams resting on elastic foundation. Compos Struct 2014; 112:292-307.
[28] Kuang J H; Chen C J. Dynamic characteristics of shaped micro-actuators solved using the differential quadrature method. J Micromech Microeng 2004; 14:647-655.
[29] Mobki H, Rezazadeh G, Sadeghi M, Vakili-Tahami F. A comprehensive study of stability in an electro-statically actuated micro-beam. Int J Non-Linear Mech 2013; 48:78-85.
[30] Lamoreaux S K. The Casimir force: background, experiments, and applications. Reports Progress Phy 2005; 68:201-236.
[31] Ganguly P, Desiraju G R. Van der Waals and polar intermolecular contact distances: Quantifying supramolecular synthons Chem Asian J 2008; 3:868-880.
[32] Reddy J N. Analysis of functionally graded plates. Int J Numer Methods Eng 2008; 47:663-684.
[33] Reddy J N, Chin C D. Thermoelastical analysis of functionally graded cylinders and plates. Therm Stresses 1998; 21:593-626.
[34] Touloukian Y S. Thermophysical Properties of High Temperature solid Materials. McMillan, 1967.
[35] Gibson L J, Ashby M F, Karam G N, Wegst U, Shercliff H R. Mechanical properties of natural materials. II. Microstructures for mechanical efficiency. Proceedings of the Royal Society of London Series A 1995; 450:141-162.
[36] Shu C. Differential quadrature and its application in engineering. Springer-Verlag London Limited; 2000.
[37] Batra R C, Porfiri M, Spinello D. Reduced-order models for microelectromechanical rectangular and circular plates incorporating the Casimir force. Int J Solids Struct 2008; 45: 3558-3583.